Energetics and kinetics of the $c(2 \times 2)$ to $(2\sqrt{2} \times \sqrt{2})R45^\circ$ transition during the early stages of Cu(100) oxidation

Minyoung Lee and Alan J. H. McGaughey
Department of Mechanical Engineering, Carnegie Mellon University, Pittsburgh, Pennsylvania 15213, USA
(Received 2 February 2011; published 29 April 2011)

The energetics and kinetics of the $c(2 \times 2)$ to $(2\sqrt{2} \times \sqrt{2})R45^\circ$ missing-row reconstruction transition on the Cu(100) surface are investigated using density functional theory calculations. First, oxygen-molecule-induced surface restructuring on the unreconstructed Cu(100) surface is compared to that on the missing-row reconstructed surface. We find that the surface-oxide energy decrease on the missing-row reconstruction (-0.149 eV/Å^2) is larger than that on the unreconstructed surface (-0.080 eV/Å^2). Cu_2O-like structures, which are found on the reconstructed surface, are not found on the unreconstructed surface. These results indicate that the missing-row reconstruction is necessary for the formation of Cu_2O on the Cu(100) surface. Then, we investigate copper ejection from the $c(2 \times 2)$ phase using the nudged elastic band method. A series of ejections onto the nearest-neighbor copper atom is found to be the most probable mechanism for the formation of the missing row. The barriers for the subsequent copper diffusion events are comparable to those on the perfect $c(2 \times 2)$ phase and the clean copper surface, suggesting that the $c(2 \times 2)$ phase acts as a copper diffusion channel during surface oxidation.

DOI: 10.1103/PhysRevB.83.165447 PACS number(s): 81.16.Pr, 68.47.Gh, 68.43.Bc, 68.35.B−

I. INTRODUCTION

During the early stages of Cu(100) oxidation, the $c(2 \times 2)$ phase is experimentally observed to transition into the $(2\sqrt{2} \times \sqrt{2})R45^\circ$ phase by a missing-row reconstruction at an oxygen coverage of around 0.5 monolayers (ML).[1–11] Based on their scanning tunneling microscopy (STM) observations, Jensen *et al.* proposed that the missing row forms by the ejection of every fourth row of the top copper layer.[2] This mechanism has been supported by experimental and computational investigations.[4,5,8,9,11–19] The stabilities of the $c(2 \times 2)$ and $(2\sqrt{2} \times \sqrt{2})R45^\circ$ phases at an oxygen coverage of 0.5 ML at zero temperature and zero pressure have been compared using density functional theory– (DFT-)predicted chemisorption energies, average oxygen atom binding energies, and surface-oxide energies.[13,17–19] The $(2\sqrt{2} \times \sqrt{2})R45^\circ$ phase is consistently found to be more stable than the $c(2 \times 2)$ phase, but the energy differences are small (e.g., 0.002 eV/Å^2 for the surface-oxide energy[19]). Iddir *et al.* used *in situ* surface x-ray scattering to investigate the stability of oxygen-covered Cu(100) surface phases for temperatures between 300 and 1000 K and oxygen partial pressuress between 10^{-10} and 10^{-4} Torr.[14] They found that the reconstructed phases [$(2\sqrt{2} \times \sqrt{2})R45^\circ$ and a related phase that has disordered copper surface vacancies] are more stable than unreconstructed phases at oxygen partial pressure higher than 10^{-8} Torr. They also found that the transition between the unreconstructed phases and the reconstructed phases is hysteretic.[14] Duan *et al.*, using first-principles atomistic thermodynamics, also found that the reconstructed phases are more stable than the unreconstructed phases (clean and 0.25 ML oxygen covered surfaces) in the same range of oxygen partial pressure.[18]

Two driving forces for the missing-row reconstruction have been suggested: (i) surface stress[4,12] and (ii) long-range Coulombic interactions.[11] Harrison *et al.* found that the compressive stress on the $c(2 \times 2)$ phase is larger than that on the $(2\sqrt{2} \times \sqrt{2})R45^\circ$ phase from both experiments (crystal curvature technique in an ultrahigh-vacuum chamber) and DFT calculations.[12] Using temperature-dependent surface-extended x-ray-absorption fine structure measurements, Lederer *et al.* also studied the $c(2 \times 2)$ and $(2\sqrt{2} \times \sqrt{2})R45^\circ$ phases.[4] They found that adsorbate-induced forces between top-layer copper atoms in the $c(2 \times 2)$ phase induce surface strains and lead to the missing-row reconstruction. They also found that the copper-oxygen bond is ionic on the unreconstructed surface but covalent on the missing-row reconstructed surface. Calculating surface Madelung potentials within the muffin-tin approximation, Stolbov *et al.* showed that long-range Coulombic interactions among oxygen atoms of the $c(2 \times 2)$ phase make copper atoms eject, leading to the $(2\sqrt{2} \times \sqrt{2})R45^\circ$ phase, which has stronger pO-dCu covalent coupling.[11] Integrating these findings, we hypothesize that long-range Coulombic interactions induce the compressive surface stress, leading to the copper atom ejection.

While the driving forces behind the missing-row reconstruction have been investigated, three fundamental questions remain. First, is the missing-row reconstruction necessary for Cu(100) oxidation? Previous investigations showed that the $(2\sqrt{2} \times \sqrt{2})R45^\circ$ phase is more stable than the $c(2 \times 2)$ phase, but did not show whether copper I oxide (Cu_2O) can form on unreconstructed Cu(100) surfaces.[13,18,19] Second, how do the copper atoms eject and diffuse away during the missing-row reconstruction? The transition kinetics from the $c(2\times2)$ phase to the $(2\sqrt{2} \times \sqrt{2})$R45° phase are not well understood. Third, where do the ejected copper atoms go? Based on STM measurements, it was suggested that the ejected copper atoms diffuse away from the missing row and attach on top of adjacent missing-row reconstructions[20] and/or on step edges at phase boundaries.[16] The diffusion paths, however, are unknown.

Here, we will focus on the first two questions by investigating the $c(2 \times 2)$ to $(2\sqrt{2} \times \sqrt{2})$R45° transition using DFT calculations. In Sec. II, the computational unit cells, setup, and procedures are presented. In Sec. III, we demonstrate, using both energetic and structural arguments, that the $c(2 \times 2)$ to $(2\sqrt{2} \times \sqrt{2})R45^\circ$ transition is necessary for subsequent

Cu_2O formation. In Sec. IV, we predict the energy barriers for copper atom ejection and diffusion during the $c(2 \times 2)$ to $(2\sqrt{2} \times \sqrt{2})R45^\circ$ transition. The results are used to propose a mechanism by which the missing-row reconstruction occurs.

II. CALCULATION METHODOLOGY

We perform the DFT calculations using the Vienna *ab initio* simulation package (VASP),[21–25] which uses a plane-wave basis set.[23,25] We use ultrasoft pseudopotentials, the Perdew-Wang 1991 (PW91) generalized gradient approximation,[26] and a 350 eV plane-wave energy cutoff. The $p(2 \times 2)$, $p(2\sqrt{2} \times \sqrt{2})$, $p(2\sqrt{2} \times 2\sqrt{2})$, and $p(4 \times 4)$ unit cells were initially considered. We found that the $p(4 \times 4)$ unit cell is required to eliminate size effects brought about by the periodic images. All $p(4 \times 4)$ slab structures include five copper layers (the bottom layer is fixed) and the vacuum gap size is 11 Å. There are 81 copper and 8 oxygen atoms in the unreconstructed $p(4 \times 4)$ unit cell, the biggest that we consider. The k-point mesh is $6 \times 6 \times 1$ and is generated by the Monkhorst-Pack scheme.[27] The k-point mesh, the energy cutoff, and the number of copper layers are chosen based on convergence tests performed for the $p(2\sqrt{2} \times 2\sqrt{2})$ missing-row reconstructed surface, which we reported previously.[19]

The stabilities of the relaxed structures described in Secs. III and IV are compared using the surface-oxide energy E_S:[17,19,28]

$$E_S = \frac{1}{A_{\text{surf}}}\left[E_{\text{O/Cu}} - N_{\text{Cu}}E_{\text{Cu,bulk}} - N_{\text{O}}\frac{E_{\text{O}_2}}{2}\right]. \quad (1)$$

Here, $E_{\text{O/Cu}}$ is the total system energy, $E_{\text{Cu, bulk}}$ is the energy of one atom in bulk fcc copper, and E_{O_2} is the energy of an isolated oxygen molecule. N_{O} and N_{Cu} are the total number of oxygen and copper atoms in the system and A_{surf} is the unit cell surface area. Because the surface-oxide energy is normalized by the unit cell area, it can be used to compare surfaces with different unit cell sizes. A spin-polarized DFT calculation is used to obtain E_{O_2}. Spin-averaged calculations are used for all other calculations.

To investigate the ejection of copper atoms and their subsequent diffusion during the $c(2 \times 2)$ to $(2\sqrt{2} \times \sqrt{2})R45^\circ$ transition, the climbing image nudged elastic band (NEB) method is applied.[29–32] The NEB method is a computational approach for finding the minimum energy path between specified initial and final equilibrium states. To specify the initial and final states, separate single-point DFT calculations are performed to ensure relaxed structures. We use five images between the initial and final states.

III. OXYGEN-INDUCED SURFACE RESTRUCTURING ON UNRECONSTRUCTED Cu(100) SURFACES

To determine if the missing-row reconstruction is a necessary state in the early stages of Cu(100) oxidation, we will investigate the stabilities and structural changes of unreconstructed Cu(100) surfaces exposed to additional oxygen molecules. We previously performed a similar study on reconstructed surfaces.[19] To examine the changes of surface stability and structure as the oxygen coverage increases, it is not sufficient to only consider an initial oxygen coverage of 0.5 ML, as done previously.[13,18] We therefore relaxed unreconstructed Cu(100) surfaces at 0.25, 0.5, and 0.75 ML oxygen coverages with an oxygen molecule located at the initial positions shown in Fig. 1(a). Although an oxygen coverage of 0.75 ML is not observed by experiments, we believe that it can exist locally.

We previously used DFT calculations to predict the energy barriers for oxygen embedding into unreconstructed surfaces. For oxygen coverages of 0.25, 0.5, and 0.75 ML, the energy barriers are 2.65, 2.37, and 0.49 eV.[17] Based on these results, we will only consider subsurface oxygen for 0.75 ML oxygen coverage. For the subsurface site, we use the octahedral site on the second copper layer, as shown in Fig. 1(b).

As presented in Table I, at 0.25 and 0.5 ML oxygen coverages, an extra oxygen molecule causes the surface-oxide energy [Eq. (1)] to increase except for one case (0.25 ML,

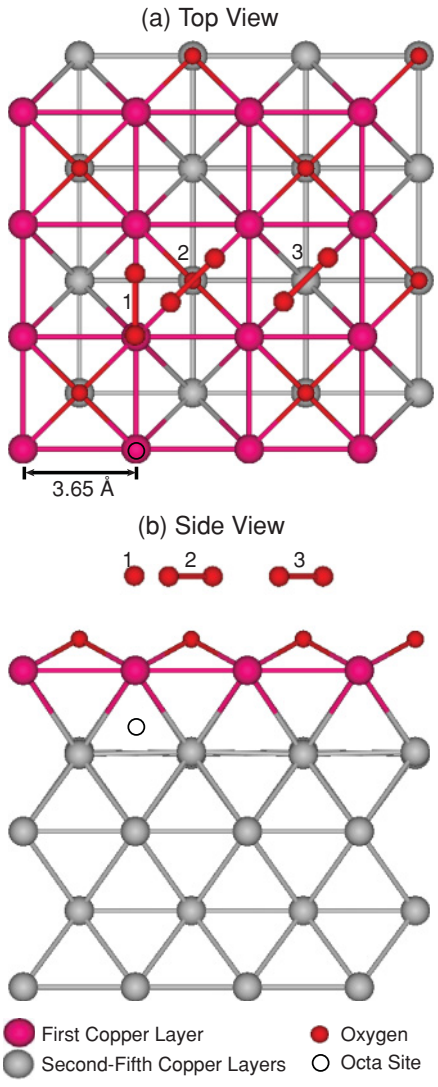

FIG. 1. (Color online) Initial positions of the oxygen molecule on the unreconstructed Cu(100) surface before structural relaxation. (a) Top and (b) side views of the unreconstructed $p(4 \times 4)$ unit cell at 0.5 ML oxygen coverage. The initial positions are labeled: (1) Top-bridge (TB), (2) fcc hollow (FCC), and (3) unoccupied fcc hollow (UFC). There are 16 octahedral (octa) sites in the subsurface region, one of which is shown.

TABLE I. Surface-oxide energy E_S of unreconstructed $p(4 \times 4)$ Cu(100) surfaces relaxed without and with an additional oxygen molecule. For each oxygen coverage, the configuration of surface oxygen atoms is chosen so as to minimize the energy [i.e., $c(2 \times 2)$ phase for 0.5 ML oxygen coverage]. The initial positions of the additional oxygen molecule are the top-bridge (TB), fcc hollow (FCC), and unoccupied fcc hollow (UFC) sites [see Fig. 1(a)]. — indicates no data. The unit cell area is 106.58 Å^2.

On-surface coverage (ML)	Subsurface coverage (ML)	E_S (eV/Å^2) No O_2	TB	FCC	UFC
0	0	0.184	—	—	—
0.25	0	0.109	0.109	0.118	0.104
0.50	0	0.047	0.053	0.056	0.052
0.75	0	0.047	0.025	0.040	0.037
0.6875	0.0625	0.032	0.024	0.024	0.022
0.75	0.25	−0.027	−0.033	−0.031	−0.029
0.75	0.50	−0.016	−0.029	−0.031	−0.027

UFC), where there is a slight decrease. For an oxygen coverage of 0.75 ML, however, the surface-oxide energy of surfaces with an oxygen molecule (TB, FCC, and UFC) is smaller than that of the surface without an oxygen molecule (No O_2). The surface-oxide energy decreases (i.e, the stability increases) because of the surface restructuring induced by the oxygen molecule. For on-surface coverage of 0.6875 ML, one of the surface-adsorbed oxygen atoms at 0.75 ML oxygen coverage was placed into the subsurface region. The surface-oxide energy of this structure is smaller than that of 0.75 ML, indicating that subsurface oxygen contributes to the structural stability. The smallest surface-oxide energy is found for an on-surface coverage of 0.75 ML and a subsurface coverage of 0.25 ML and the oxygen molecule initially at the TB site. We note, however, that all cases with 0.25 ML subsurface oxygen have a much smaller surface-oxide energy than those without.

After the surface restructuring on the unreconstructed Cu(100) surfaces at 0.75 ML oxygen coverage with or without subsurface oxygen, the top copper layer is elevated and tetrahedral copper-oxygen structures exist. The Cu-O-Cu and O-Cu-O angles range from 93.18° to 132.15° and the Cu-O bond lengths range from 1.883 to 2.388 Å. These tetrahedral structures do not have the characteristics of Cu_2O [our DFT-predicted (PW91) Cu-O-Cu and O-Cu-O bond angles are 109.471° and 180°, and the Cu-O bond length is 1.849 Å]. We also added two oxygen molecules to the unreconstructed surface at 0.75 ML oxygen coverage, but no Cu_2O-like structures were produced. In contrast, we previously showed that surface restructuring induced by an additional oxygen molecule on the missing-row reconstructed Cu(100) surface can produce Cu_2O-like structures with comparable bond angles and lengths to that of Cu_2O when there is subsurface oxygen.[19]

Based on these results and those presented in our previous report,[19] there are two potential oxidation paths starting from the $c(2 \times 2)$ phase (see Fig. 2). The first path is through the unreconstructed surfaces at an on-surface coverage of 0.75 ML with subsurface oxygen followed by further oxygen exposure. The second path is through missing-row reconstruction at an on-surface oxygen coverage of 0.5 ML with subsurface oxygen followed by further oxygen exposure. The surface-oxide energy eventually decreases along both paths, but the magnitude of the drop is bigger through the missing-row reconstruction path (−0.149 eV/Å^2) than through the unreconstructed path (−0.080 eV/Å^2). This result indicates that the missing-row reconstructed path enhances the structural stability more than the unreconstructed path. Previous investigations did not capture this result because they fixed the oxygen coverage at 0.5 ML.[13,18] Based on these energetics and structural arguments, we believe that the missing-row reconstruction is a highly probable step for Cu_2O nucleation during Cu(100) oxidation.

IV. $C(2 \times 2)$ to $(2\sqrt{2} \times \sqrt{2})R45°$ TRANSITION

A. Copper atom ejection

To investigate the energetics and kinetics of the copper ejection, we will propose a set of potential paths and then compare their energy barriers. The initial (A) and final positions (B, C, and D) of the copper atom in the three

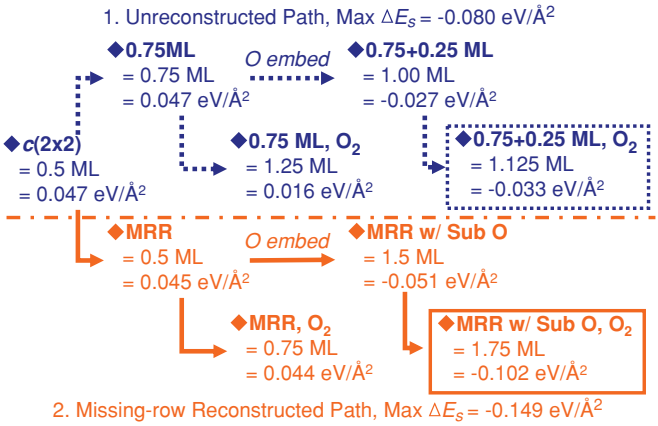

FIG. 2. (Color online) Potential oxidation paths on the unreconstructed and missing-row reconstructed Cu(100) surfaces. The surface-oxide energies (E_S) are calculated from the $p(4 \times 4)$ unit cell for the unreconstructed path and from the $p(2\sqrt{2} \times 2\sqrt{2})$ unit cell for the missing-row reconstructed path (Ref. 19). The surface-oxide energies are presented in Table I for the unreconstructed path. "0.75 + 0.25 ML" indicates an on-surface coverage 0.75 ML and a subsurface coverage 0.25 ML. For the missing-row reconstructed path, "MRR" denotes the missing-row reconstructed Cu(100) surface and "MRR w/ Sub O" denotes the missing-row reconstructed Cu(100) surface with subsurface oxygen. The structures with an oxygen molecule are denoted with O_2.

possible initial ejection paths from the $c(2 \times 2)$ phase are shown in Figs. 3(a) and 3(b). Relaxed configurations of these structures are used in the NEB calculations. The energetics are shown in Fig. 3(c) and reported in Table II. The energy

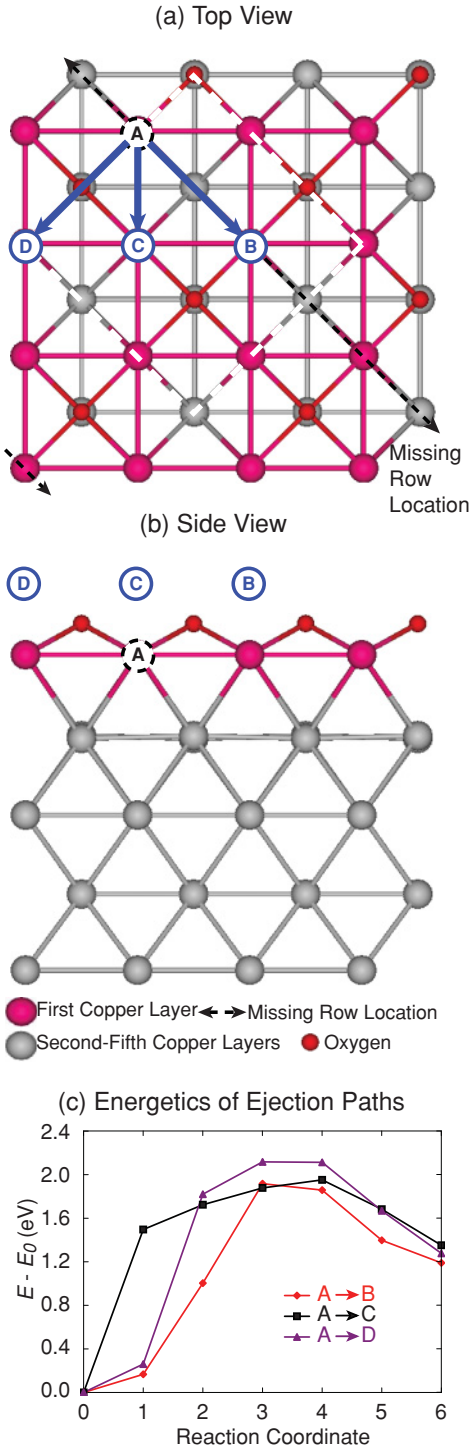

FIG. 3. (Color online) (a) Top view and (b) side view of the $p(4 \times 4)$ unit cell showing the initial (A) and final positions (B, C, and D) for copper ejection (the structures shown here are unrelaxed). For reference, the $p(2\sqrt{2} \times 2\sqrt{2})$ unit cell is contained by the white dashed line in (a). (c) Energetics of copper ejection (E = image energy, E_0 = energy of image 0); see Table II.

TABLE II. Energy difference E_{diff} and energy barrier E_{barrier} for the copper ejection paths shown in Figs. 3(a), 4(a), 4(b), 4(c), and 5(a).

Index	E_{diff} (eV)	E_{barrier} (eV)
$A \rightarrow B$	1.19	1.92
$A \rightarrow C$	1.35	1.95
$A \rightarrow C$ w/ V&Ad	0.62	1.41
$A \rightarrow C$ w/ V	1.58	1.66
$(A \rightarrow C) \times 2$	1.97	2.47
$A \rightarrow D$	1.28	2.12
$A \rightarrow D$ w/ V&Ad	1.33	2.03
$A \rightarrow D$ w/ V	1.28	2.12
$(A \rightarrow D) \times 2$	2.60	3.23

barriers are comparable, ranging from 1.92 eV ($A \rightarrow B$) to 2.12 eV ($A \rightarrow D$). We note that the B site lies on what would be the missing row. The only relevant next event is therefore a diffusion to a C or D site, which is discussed in Sec. IV B. The magnitudes of these barriers are comparable to the activation energy of Cu_2O formation on the Cu(100) surface (1.4 ± 0.2 eV),[33] and to the activation energy for Ag on the (Ag 1 ML)/Mo(100) surface (2.5 eV).[34]

Once one copper atom has been ejected, the question arises as to what happens next. Does a second copper atom eject while the first is still nearby? Or does the first atom diffuse away before the second atom ejects? Or can two copper atoms eject at the same time? We investigated these possibilities using the ejection paths shown in Figs. 4(a) [ejection with vacancy and adatom (w/ V&Ad)], 4(b) [ejection with vacancy (w/ V)], and 4(c) [coordinated ejection ($\times 2$)]. The energy barriers are provided in Table II. The energy barriers of all the $A \rightarrow D$ paths are similar. We believe that the $A \rightarrow D$ paths are not affected by the adatom or vacancy because they all go over an oxygen atom. Large structural changes result, which supersede any effect of the adatom or vacancy. When the first ejected copper atom stays at the C site (on top of the nearest-neighbor copper atom) and the second copper atom ejects ($A \rightarrow C$ w/ V&Ad), the energy barrier decreases from 1.95 to 1.41 eV. The initial state to final state energy difference (E_{diff}) of the $A \rightarrow C$ w/ V&Ad ejection is much smaller than those of the other ejection paths (see Table II). In the final state of the $A \rightarrow C$ w/ V&Ad ejection, an O-Cu-O-Cu-O chain is found along the missing-row direction, which is not found in the other cases. If the first ejected copper atom diffuses away ($A \rightarrow C$ w/ V), the energy barrier for the second copper ejection near the vacancy decreases to 1.66 eV. These results suggests that once one copper atom is ejected through any of the three initial paths, many copper atoms will soon follow on $A \rightarrow C$ paths. The continuous ejection of an entire row is consistent with experimental observations.[1,2,6]

The coordinated ($\times 2$) and noncoordinated with vacancy and adatom ejections ($A \rightarrow C$ followed by $A \rightarrow C$ w/V&Ad) ejections lead to the same final structure. As shown in Fig. 5(a), there are two energy barriers for the noncoordinated ejection and one energy barrier for the coordinated ejection. To determine which event is more probable, we use transition state theory (TST), a theoretical method for calculating

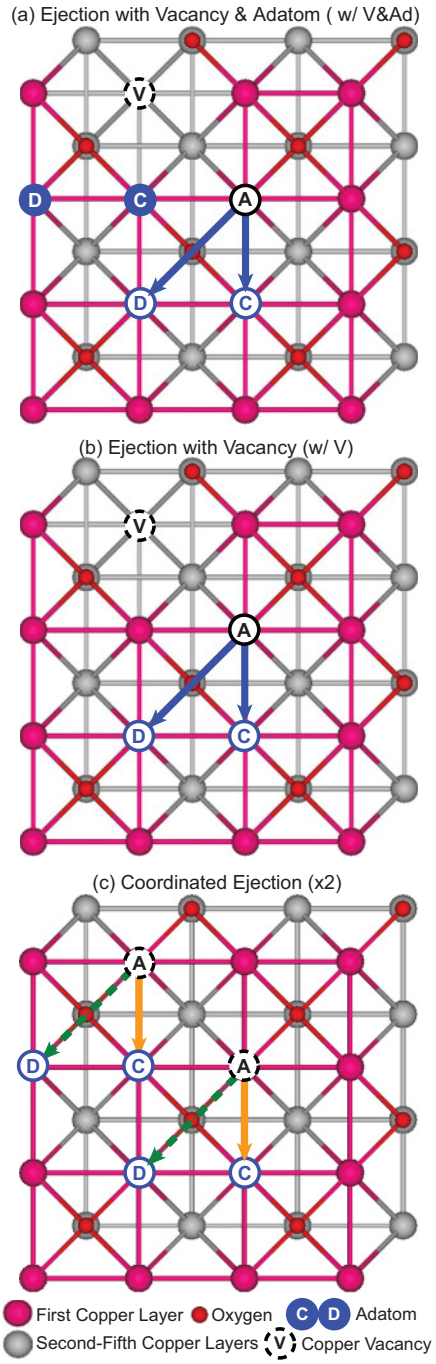

FIG. 4. (Color online) Three possibilities for the second copper ejection: (a) with vacancy and adatom (w/ V&Ad), (b) with vacancy (w/ V), and (c) coordinated ejection (two neighboring copper atoms eject at the same time, $\times 2$). The energy barriers are provided in Table II.

the transition rate between two equilibrium states using thermodynamics, kinetic theory, and statistical mechanics.[35,36] The transition rate can be calculated under the harmonic approximation as

$$k_{\text{path}}^{TST,H} = \nu_0 \exp\left[-\frac{E_{\text{barrier}}}{k_B T}\right], \tag{2}$$

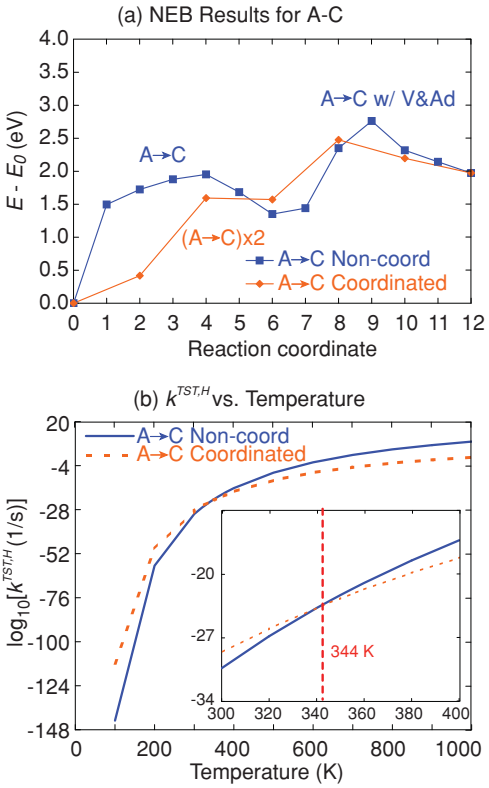

FIG. 5. (Color online) Comparing the energetics of coordinated and noncoordinated copper atom ejection for the $A \rightarrow C$ path. (a) Reaction pathways. (b) Transition rates vs temperature. The energy barriers are provided in Table II. The noncoordinated ejection is more probable than the coordinated ejection at temperatures higher than 344 K.

where ν_0, k_B, and T are the atomic vibrational frequency, the Boltzmann constant, and the temperature.[37] We take ν_0 to be 1.0×10^{13} [Hz], the typical period of an atomic vibration.[38] The transition rates of the noncoordinated ($A \rightarrow C$ followed by $A \rightarrow C$ w/ V&Ad) and coordinated [$(A \rightarrow C)\times 2$] ejections are $k_{A\rightarrow C}^{TST,H}$ $k_{A\rightarrow C\ w/\ V\&Ad}^{TST,H}$ and $k_{(A\rightarrow C)\times 2}^{TST,H}$, and are plotted versus temperature in Fig. 5(b). The most probable ejection mechanism changes from the coordinated ejection to the noncoordinated ejection at 344 K for the $A \rightarrow C$ paths and at 356 K for the $A \rightarrow D$ paths (not shown). Experimental observations of Cu(100) oxidation have all been done at temperatures higher than 450 K.[2,6,14,39] Our results suggest that the missing-row reconstruction observed in these experiments is produced by noncoordinated ejections.

Based on the results presented in this section, we believe that the missing row forms through $A \rightarrow C$ ejections once the initial copper atom has ejected. In the next section, we will investigate the subsequent diffusion processes.

B. Copper atom diffusion

We now examine the copper diffusion events that will follow the copper ejection, again using the NEB method. All the energy differences and barriers are provided in Table III. Because the ejection barriers for the first ejection are comparable for all three paths, we also investigate diffusion from the B and D sites. As shown in Fig. 6(b), there are

TABLE III. Energy difference E_{diff} and energy barrier E_{barrier}, for copper diffusion paths during the transition from the $c(2 \times 2)$ to the missing-row reconstructed Cu(100) surface. The copper diffusion paths are shown in Figs. 6(a) and 6(b) for diffusion following the copper ejection and in Fig. 6(c) for diffusion on the perfect $c(2 \times 2)$ phase.

Path	E_{diff} (eV)	E_{barrier} (eV)
$C1 \rightarrow$ I	0.58	0.99
$C1 \rightarrow$ II	−0.59	0.41
$C2 \rightarrow$ II	0.72	0.87
$C2 \rightarrow$ III	0.33	1.52
$D \rightarrow C$	0.07	0.56
$B \rightarrow B/D \rightarrow D$	0.09	0.64
$B \rightarrow C$	−0.13	0.52
$B \rightarrow D/D \rightarrow B$	0.00	0.97
Perfect $c(2 \times 2)$ phase		
α	0	0.63
β	0	0.55
γ	0	0.74

four distinct diffusion paths ($B \rightarrow B$, $B \rightarrow C$, $B \rightarrow D$, and $D \rightarrow C$). Note that $D \rightarrow D$ and $D \rightarrow B$ are equivalent to $B \rightarrow B$ and $B \rightarrow D$. To investigate the diffusion away from C sites (see Fig. 4 and Table II), there are four diffusion paths ($C1 \rightarrow$ I, $C1 \rightarrow$ II, $C2 \rightarrow$ II, $C2 \rightarrow$ III), as shown in Fig. 6(a). We studied the $C2 \rightarrow$ I path but found that the copper adatom at the $C1$ site returned to $V1$ because of the periodicity of the computational cell. We also investigated copper diffusion on the perfect $c(2 \times 2)$ phase as shown in Fig. 6(c) (paths α, β, and γ).

To increase the probability of the second copper ejection, as discussed in Sec. IV A, a copper atom needs to be at a C site. Although a copper atom may initially eject to a B or D site, it can diffuse to a C site through $B \rightarrow C$ or $D \rightarrow C$. The energy barriers of the $B \rightarrow C$ and $D \rightarrow C$ diffusions are smaller than all the ejection barriers and the other diffusion barriers (see Tables II and III), such that there will be a source of atoms available to promote further ejection.

From the C sites, the $C1 \rightarrow$ II path has, by far, the smallest energy barrier (0.41 eV). The $C2 \rightarrow$ III path has a much higher energy barrier because the diffusion is over an oxygen atom (this barrier may also be affected by the periodic image of $V1$). Although these energy barriers may be influenced by our computational limitations (i.e., the periodicity of unit cell), the energy barrier of the $C1 \rightarrow$ II path is clearly smaller than the others. The $C1 \rightarrow$ II path also has a negative energy difference (E_{diff}), indicating that the copper diffusion along the $C1 \rightarrow$ II path is energetically favorable. One possible explanation for this result is that in the final state of the $C1 \rightarrow$ II path, there are two copper atoms at the nearest-neighbor distance (i.e., at the II and $C2$ sites), leading to a low-energy Cu-Cu cluster. We can thus choose the $C1 \rightarrow$ II path as the most probable diffusion path following $A \rightarrow C$ ejections.

If we ignore the copper vacancy [V in Fig. 6(b)], the $B \rightarrow B$, $B \rightarrow C$, and $B \rightarrow D$ paths are equivalent to the α, β, and γ paths on the $c(2 \times 2)$ phase [see Figs. 6(b) and 6(c)]. The energy barriers for $B \rightarrow B$ and $B \rightarrow C$ are within 0.03 eV of those for the α and β paths (i.e., the vacancy does not play a role). The $B \rightarrow D$ and γ paths, however, have a 0.23 eV

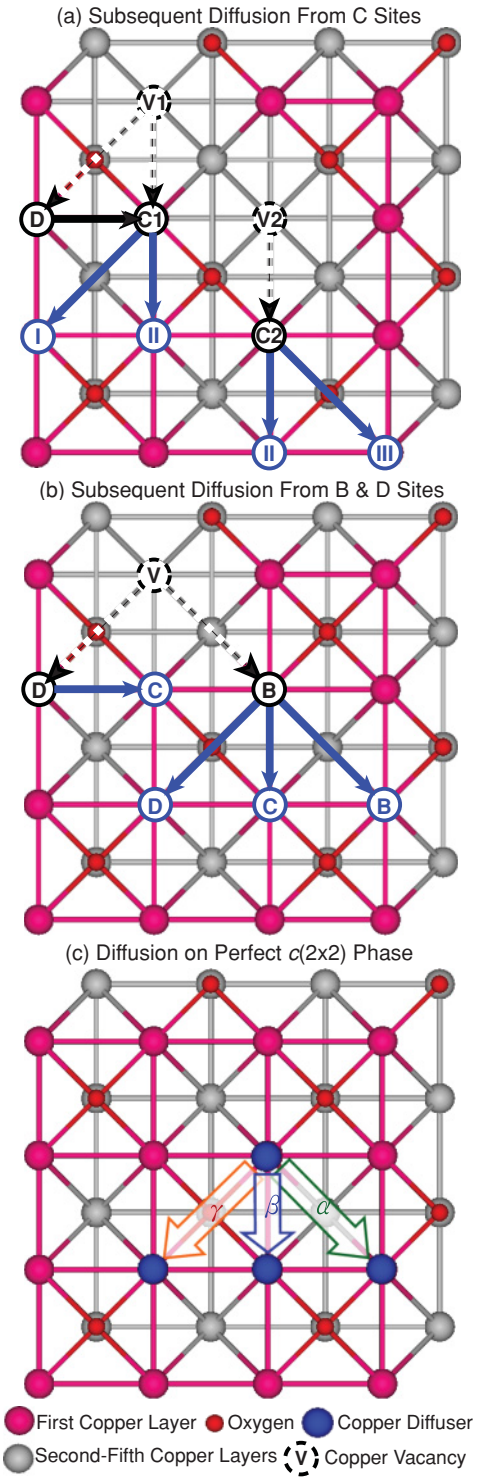

FIG. 6. (Color online) Copper diffusion paths following the copper ejection from (a) C sites and (b) B and D sites. V is the copper vacancy, which is the original location of the ejected copper atom. The dashed arrows are the ejection paths and the solid arrows are the diffusion paths. (c) Copper diffusion paths (α,β,γ) on the perfect $c(2 \times 2)$ phase. Path γ is over an oxygen atom. There is no oxygen atom along path α.

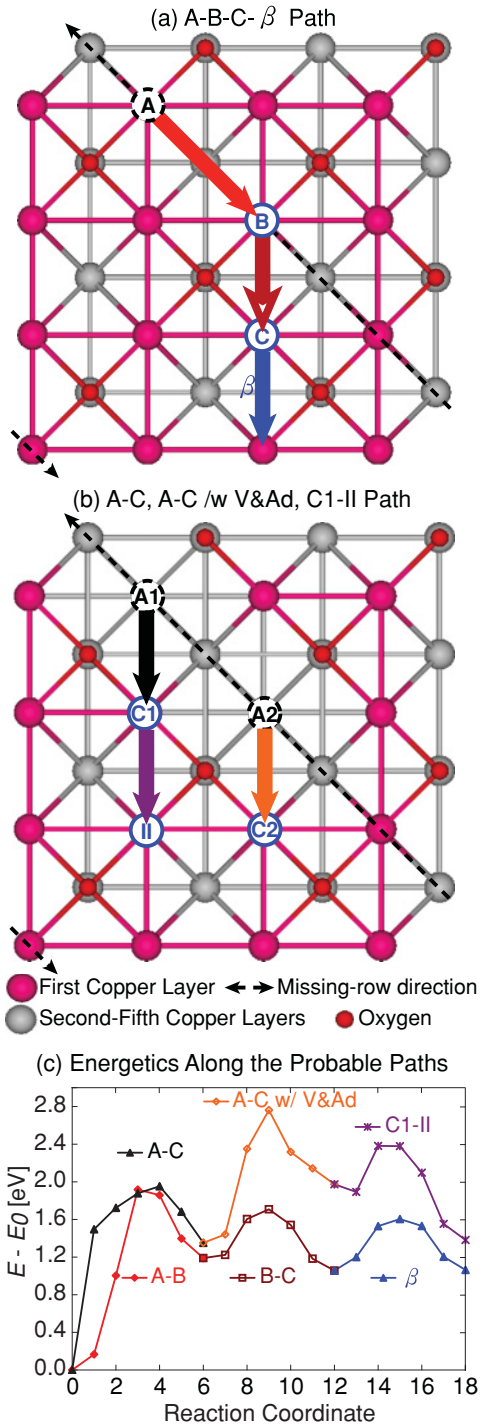

FIG. 7. (Color online) Probable copper ejection and diffusion paths during the transition from $c(2 \times 2)$ to $(2\sqrt{2} \times \sqrt{2})R45^\circ$ on the Cu(100) surface (the original positions of the ejected copper atoms are indicated by dashed circles). (a) $A \rightarrow B \rightarrow C$-$\beta$ path, and (b) $A1 \rightarrow C1$–$A2 \rightarrow C2$ w/ V&Ad–$C1 \rightarrow$ II path. Note that the β path can be perpendicular to the β path shown in (a). (c) NEB results for each path.

difference in their energy barriers. In the $B \rightarrow D$ path, the vacancy breaks the symmetry of the surface, leading to the energy barrier difference.

On the perfect $c(2 \times 2)$ phase, the β path has the smallest barrier, 0.55 eV, which is comparable to copper diffusion barriers on the clean Cu(100) surface measured from experiment (0.36 ± 0.03 eV),[34] and predicted from a previous DFT study (0.53 eV).[40] This result indicates that the mobility of a copper adatom near the missing row is similar to that on the clean and $c(2 \times 2)$ oxygen-covered Cu(100) surfaces. The $c(2 \times 2)$ phase can thus play an important role as a copper diffusion channel, consistent with the experimental findings of Lahtonen *et al.*[16]

C. Most probable paths

Although we did not consider all possible ejection and diffusion paths, we tried to follow a logical sequence of these events. In summary, likely sequences of copper ejection and diffusion are shown in Figs. 7(a) and 7(b). In the path shown in Fig. 7(a), a copper atom ejects from A to B, then diffuses to C, and finally diffuses away from the vacancy through the β diffusion path on the perfect $c(2 \times 2)$ phase. In the path shown in Fig. 7(b), there are two ejected copper atoms. The first copper atom ejects from $A1$ to $C1$ and stays there, decreasing the energy barrier for the second copper atom ejection (or another copper atom can diffuse to $C1$). With the copper adatom on $C1$, the second copper atom ejects from $A2$ to $C2$. Finally, the first copper atom diffuses from $C1$ to II. The results shown in Fig. 7(c) describe the energy surface that the ejected copper atom goes through in these two paths. The energies of the final states are much bigger than that of the initial state [the $c(2 \times 2)$ phase] because the NEB method must be applied to initial and final states that include the same number of atoms (i.e., the ejected copper atoms from the missing-row remain in the unit cell). To check if our results are reasonable, we removed copper atoms one by one from a potential missing row on the $c(2 \times 2)$ phase. The surface-oxide energy decreased and converged to the value for the missing-row reconstruction, indicating that the energy differences between the initial and final states shown in Fig. 7(b) are induced by the limitation of the NEB method.

V. SUMMARY

We used DFT calculations to determine if the missing-row reconstruction is necessary for Cu_2O formation on the Cu(100) surface and to investigate the kinetics and energetics of copper ejection and diffusion during the missing-row reconstruction.

In Sec. III, oxygen-molecule-induced surface restructuring on unreconstructed Cu(100) surfaces was investigated. The results were compared to similar calculations on the missing-row reconstructed Cu(100) surface. The surface-oxide energy decrease is bigger through the missing-row reconstruction than through the unreconstructed surface. The Cu_2O-like structures that we previously observed on the reconstructed surface are not observed on the unreconstructed Cu(100) surfaces. These results led to the conclusion that the missing-row reconstruction is a necessary step in the formation of Cu_2O.

In Sec. IV A, we investigated copper ejection paths using the NEB method. We found that the most probable route to the missing-row reconstruction is the successive ejection of copper atoms to top sites on the nearest-neighbor copper atoms (C site). The presence of a copper adatom on the C site

was found to reduce the energy barrier for the next ejection by 0.54 eV. In Sec. IV B, we showed that diffusion away from the *C* site is comparable to that on the $c(2 \times 2)$ phase. This finding indicates that the $c(2 \times 2)$ phase can act as a copper diffusion channel. In Sec. IV C, we summarized the probable ejection and diffusion paths.

After the missing-row reconstruction, Cu(100) oxidation proceeds with oxygen embedding,[17] copper adlayer formation,[20] and copper and copper-vacancy exchange (order-disorder transition).[14] Energy barriers for the oxygen embedding and the copper-vacancy exchange are available from previous investigations.[14,17] In the future, these energy barriers and those calculated here could be used in kinetic Monte Carlo simulations[41–45] to investigate length and time scales not accessible with DFT calculations.

ACKNOWLEDGMENTS

This work is supported by the United States Department of Energy, Office of Basic Energy Sciences, Division of Materials Science and Engineering (Grant No. DOE FGOA01ER45919). We thank Judith Yang, Wissam Al-Saidi, and Sang eun Jee for helpful discussions. We acknowledge support from the Carnegie Institute of Technology and the Department of Chemical Engineering at Carnegie Mellon University for the purchase of a computing cluster used in this work. Computational resources were provided by the Center for Molecular and Materials Simulations at the University of Pittsburgh and the National Science Foundation through TeraGrid resources provided by Texas Advanced Computing Center (Grant No. TG-DMR100088).

[1] H. C. Zeng, R. A. McFarlane, and K. A. R. Mitchell, Surf. Sci. **208**, L7 (1989).
[2] F. Jensen, F. Besenbacher, E. Laegsgaard, and I. Stensgaard, Phys. Rev. B **42**, 9206 (1990).
[3] K. W. Jacobsen and J. K. Norskov, Phys. Rev. Lett. **65**, 1788 (1990).
[4] T. Lederer, D. Arvanitis, G. Comelli, L. Troger, and K. Baberschke, Phys. Rev. B **48**, 15390 (1993).
[5] F. M. Leibsle, Surf. Sci. **337**, 51 (1995).
[6] T. Fujita, Y. Okawa, Y. Matsumoto, and K. I. Tanaka, Phys. Rev. B **54**, 2167 (1996).
[7] T. Wiell, J. E. Klepeis, P. Bennich, O. Bjorneholm, N. Wassdahl, and A. Nilsson, Phys. Rev. B **58**, 1655 (1998).
[8] D. Sekiba, T. Inokuchi, Y. Wakimoto, K. Yagi-Watanabe, and H. Fukutani, Surf. Sci. **470**, 43 (2000).
[9] M. Kittel, M. Polcik, R. Terborg, J.-T. Hoeft, P. Baumgartel, A. Bradshaw, R. Toomes, J.-H. Kang, D. Woodru, M. Pascal, C. Lamont, and E. Rotenberg, Surf. Sci. **470**, 311 (2001).
[10] S. Stolbov, A. Kara, and T. S. Rahman, Phys. Rev. B **66**, 245405 (2002).
[11] S. Stolbov and T. S. Rahman, Phys. Rev. Lett. **89**, 116101 (2002).
[12] M. J. Harrison, D. P. Woodruff, J. Robinson, D. Sander, and J. Kirschner, Phys. Rev. B **74**, 165402 (2006).
[13] N. Bonini, A. Kokalj, A. D. Corso, S. de Gironcoli, and S. Baroni, Surf. Sci. **600**, 5074 (2006).
[14] H. Iddir, D. D. Fong, P. Zapol, P. H. Fuoss, L. A. Curtiss, G.-W. Zhou, and J. A. Eastman, Phys. Rev. B **76**, 241404(R) (2007).
[15] S. Jaatinen, J. Blomqvist, P. Salo, A. Puisto, M. Alatalo, M. Hirsimaki, M. Ahonen, and M. Valden, Phys. Rev. B **74**, 075402 (2006).
[16] K. Lahtonen, M. Hirsimaki, M. Lampimaki, and M. Valden, J. Chem. Phys. **129**, 124703 (2008).
[17] M. Lee and A. J. H. McGaughey, Surf. Sci. **603**, 3404 (2009).
[18] X. Duan, O. Warschkow, A. Soon, B. Delley, and C. Stampfl, Phys. Rev. B **81**, 075430 (2010).
[19] M. Lee and A. J. H. McGaughey, Surf. Sci. **604**, 1425 (2010).
[20] M. Lampimaki, K. Lahtonen, M. Hirsimaki, and M. Valden, J. Chem. Phys. **126**, 034703 (2007).
[21] G. Kresse and J. Hafner, Phys. Rev. B **47**, 558 (1993).
[22] G. Kresse and J. Hafner, Phys. Rev. B **49**, 14251 (1994).
[23] G. Kresse and J. Hafner, J. Phys.: Condens. Matter **6**, 8245 (1994).
[24] G. Kresse and J. Furthmuller, Comput. Mater. Sci. **6**, 15 (1996).
[25] G. Kresse and J. Furthmuller, Phys. Rev. B **54**, 11169 (1996).
[26] J. P. Perdew, J. A. Chevary, S. H. Vosko, K. A. Jackson, M. R. Pederson, D. J. Singh, and C. Fiolhais, Phys. Rev. B **46**, 6671 (1992).
[27] H. J. Monkhorst and J. D. Pack, Phys. Rev. B **13**, 5188 (1976).
[28] I. Batyrev, A. Alavi, and M. W. Finnis, Faraday Discuss. **144**, 33 (1999).
[29] H. Jonsson, G. Mills, and K. W. Jacobsen, *Classical and Quantum Dynamics in Condensed Phase Simulations*, edited by B. J. Berne, G. Ciccotti, and D. F. Coker (World Scientific, Singapore, 1998).
[30] G. Henkelman, B. P. Uberuaga, and H. Jonsson, J. Chem. Phys. **113**, 9901 (2000).
[31] G. Henkelman and H. Jonsson, J. Chem. Phys. **113**, 9978 (2000).
[32] R. A. Olsen, G. J. Kroes, G. Henkelman, A. Arnaldsson, and H. Jonsson, J. Chem. Phys. **121**, 9776 (2004).
[33] J. C. Yang, M. Yeadon, B. Kolasa, and J. M. Gibson, Scr. Mater. **38**, 1237 (1998).
[34] J. A. Venables, *Introduction to Surface and Thin Film Process* (Cambridge University Press, Cambridge, 2000).
[35] H. Eyring, J. Chem. Phys. **3**, 107 (1935).
[36] K. J. Laidler and M. C. King, J. Phys. Chem. **87**, 2657 (1983).
[37] A. F. Voter, Phys. Rev. B **34**, 6819 (1986).
[38] D. S. Sholl and J. Steckel, *Density Functional Theory: A Practical Introduction* (John Wiley & Sons, New York, 2008).
[39] G. Zhou and J. C. Yang, Appl. Surf. Sci. **210**, 165 (2003).
[40] M. Alatalo, S. Jaatinen, P. Salo, and K. Laasonen, Phys. Rev. B **70**, 245417 (2004).
[41] W. M. Young and E. W. Elcock, Proc. Phys. Soc. **89**, 735 (1966).
[42] J. Venables, G. Spiller, and M. Hanbuchen, Rep. Prog. Phys. **47**, 399 (1984).
[43] P. Ruggerone, C. Ratsch, and M. Scheffler, Chem. Phys. Solid Surf. **8**, 490 (1997).
[44] D. Landau and K. Binder, *A Guide to Monte Carlo Simulation in Statistical Physics* (Cambridge University Press, Cambridge, 2003).
[45] E. Cox, M. Li, P.-W. Chung, C. Ghosh, T. S. Rahman, C. J. Jenks, J. W. Evans, and P. A. Thiel, Phys. Rev. B **71**, 115414 (2005).